# Functional Coupling of TRPM2 and Extrasynaptic NMDARs Exacerbates Excitotoxicity in Ischemic Brain Injury

Pengyu Zong[1], Jianlin Feng[1], Zhichao Yue[1], Yunfeng Li[2], Gongxiong Wu[3], Baonan Sun[1], Yanlin He[1], Barbara Miller[4], Albert S. Yu, Zhongping Su[1], Jia Xie[1], Yasuo Mori[5], Bing Hao[2], Lixia Yue[1,*]

[1] Department of Cell Biology, Calhoun Cardiology Center, University of Connecticut School of Medicine (UConn Health), Farmington, CT 06030, USA;

[2] Department of Molecular Biology and Biophysics, University of Connecticut School of Medicine (UConn Health), Farmington, CT 06030, USA;

[3] Department of Medicine, Brigham and Women's Hospital, Laboratory for Translational Research, Harvard Medical School, Cambridge, MA 02139, USA;

[4] Departments of Biochemistry and Molecular Biology, The Pennsylvania State University College of Medicine, P.O. Box 850, Hershey, Pennsylvania, 17033, USA;

[5] Laboratory of Molecular Biology, Department of Synthetic Chemistry and Biological Chemistry, Graduate School of Engineering, Kyoto University, Kyoto, 615-8510, Japan; The World Premier International Research Initiative-Institute for Integrated Cell-Material Sciences, Kyoto University, Kyoto, 615-8510, Japan.

*Corresponding author: Lixia Yue: lyue@uchc.edu

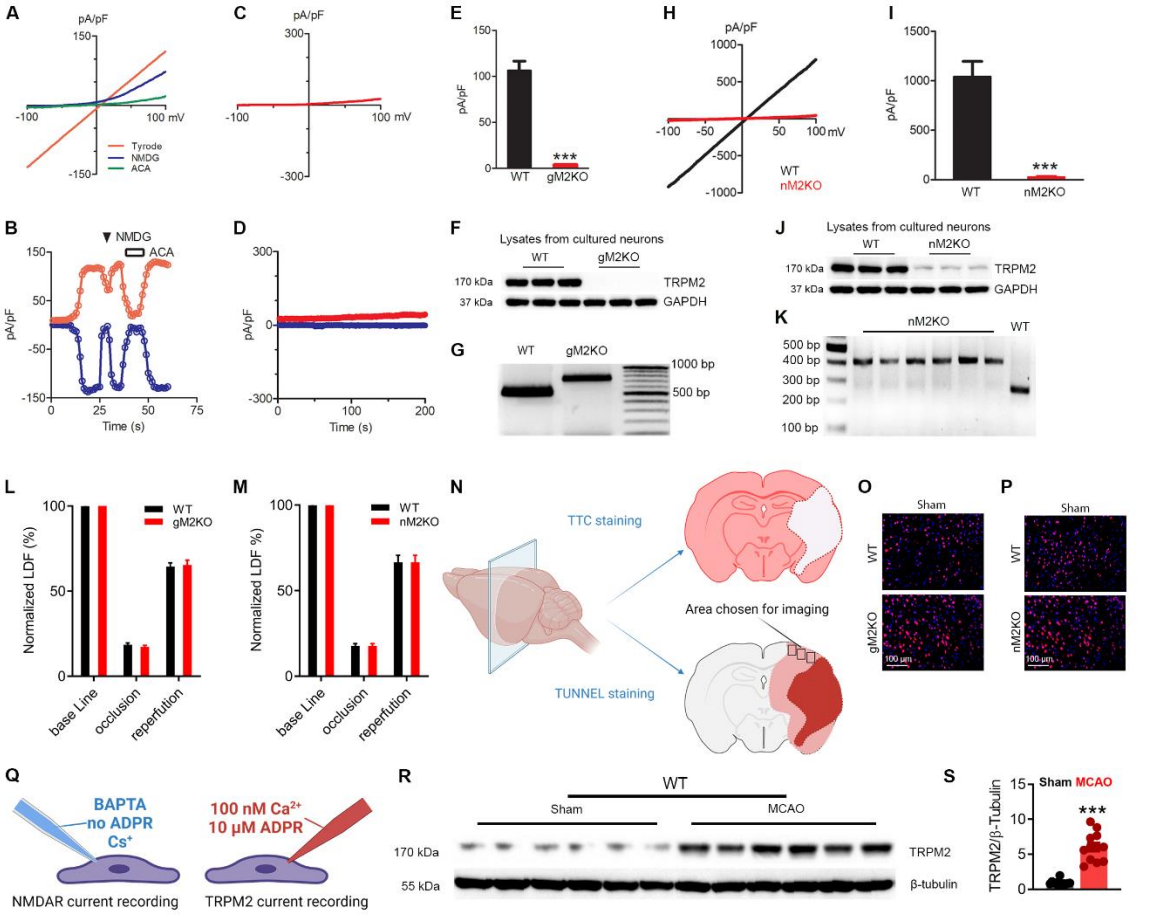


**Supplementary Figure 1 | TRPM2 currents recorded in WT neurons and determination of TRPM2 deletion in the global and neuron-specific knockout mice, Related to Figure 1**

(A-E), TRPM2 currents recorded in the cortical neurons with pipette solution containing ADPR and $Ca^{2+}$. (A, C), Representative currents elicited by a ramp protocol ranging from -100 to +100 mV in WT neurons (A) but not in global TRPM2-KO (gM2KO) neurons (C). NMDG was used to ensure no leak contamination, and ACA (30 μM) was used to inhibit TRPM2 currents. (B, D), Inward and outward current measured at -100 mV and +100 mV were plotted against time (B). No currents were recorded in the gM2KO neurons (D). (E), Average current amplitude (at +100 mV) of TRPM2 in WT neurons; TRPM2 current was eliminated in gM2KO neurons. Please note that NMDG eliminated inward TRPM2 currents (A, B), indicating no leak current, but meanwhile slightly reduced outward currents (A, B) because elimination of extracellular $Ca^{2+}$ entry will gradually close TRPM2.

(F-G), Conformation of global TRPM2 knockout (gM2KO) by genotyping (G) and WB (F). (F),

Representative WB results from 3 brains of WT and gM2KO mice. (G), Representative PCR genotyping results showing a 514 bp and 740 bp products for WT and gM2KO mice.

(H-I), Representative TRPM2 currents recorded in neurons from WT and neuron-specific TRPM2-KO (nM2KO) mice. TRPM2 currents were recorded in cortical neurons from WT neurons but not in nM2KO neurons (H). Average currents measured at +100 mV (I). Please note that nM2KO eliminated TRPM2 currents.

(J-K), Conformation of neuron-specific knockout of TRPM2 by WB and genotyping. (J), Representative WB results to detect TRPM2 deletion using cultured neurons from 3 WT and nestin-cre$^{+}$ floxed mice (nM2KO). TRPM2 protein was largely eliminated in cultured neurons of nM2KO. The trace amounts of protein detected in M2KO neuron cultures is likely from non-neuronal cells in the culture dishes. (K), Representative PCR results for genotyping of TRPM2 flox/flox expression. The predicted PCR products are 400 bp in TRPM2-flox/flox expressing mice (n-6) and 260 bp in a WT mouse as control.

(L-M), Representative data of blood flow changes measured using LDF. Blood flow was measured using LDF before and after MCAO, as well as after reperfusion. Successful MCA occlusion was confirmed by 85% reduction of cerebral blood flow OGD (***, $p < 0.001$, unpaired *t*-test, mean ± SEM; n=18 for WT and n=16 for gM2KO groups; and n=13 for WT and n=11 for nM2KO groups).

(N), Graphic illustration showing the position (Black square) of penumbra area chosen for Tunnel staining.

(O, P) Sham for the TUNNEL staining after MCAO in Figure 1E and Figure 1G, respectively.

(Q), Graphic illustration showing the recording condition for NMDAR and TRPM2 current. Activation of TRPM2 requires both $Ca^{2+}$ and ADPR, and BAPTA is the most potent $Ca^{2+}$ chelator. Therefore, TRPM2 shall not be activated when NMDAR current is being recorded. Activation of NMDAR requires its ligands (glutamate or NMDA), and can be blocked by extracellular $Mg^{2+}$. Therefore, NMDAR shall not be activated when TRPM2 is being recorded.

(R, S) Western blot analysis of TRPM2 expression in the brain from mice subjected to sham or MCAO surgery.

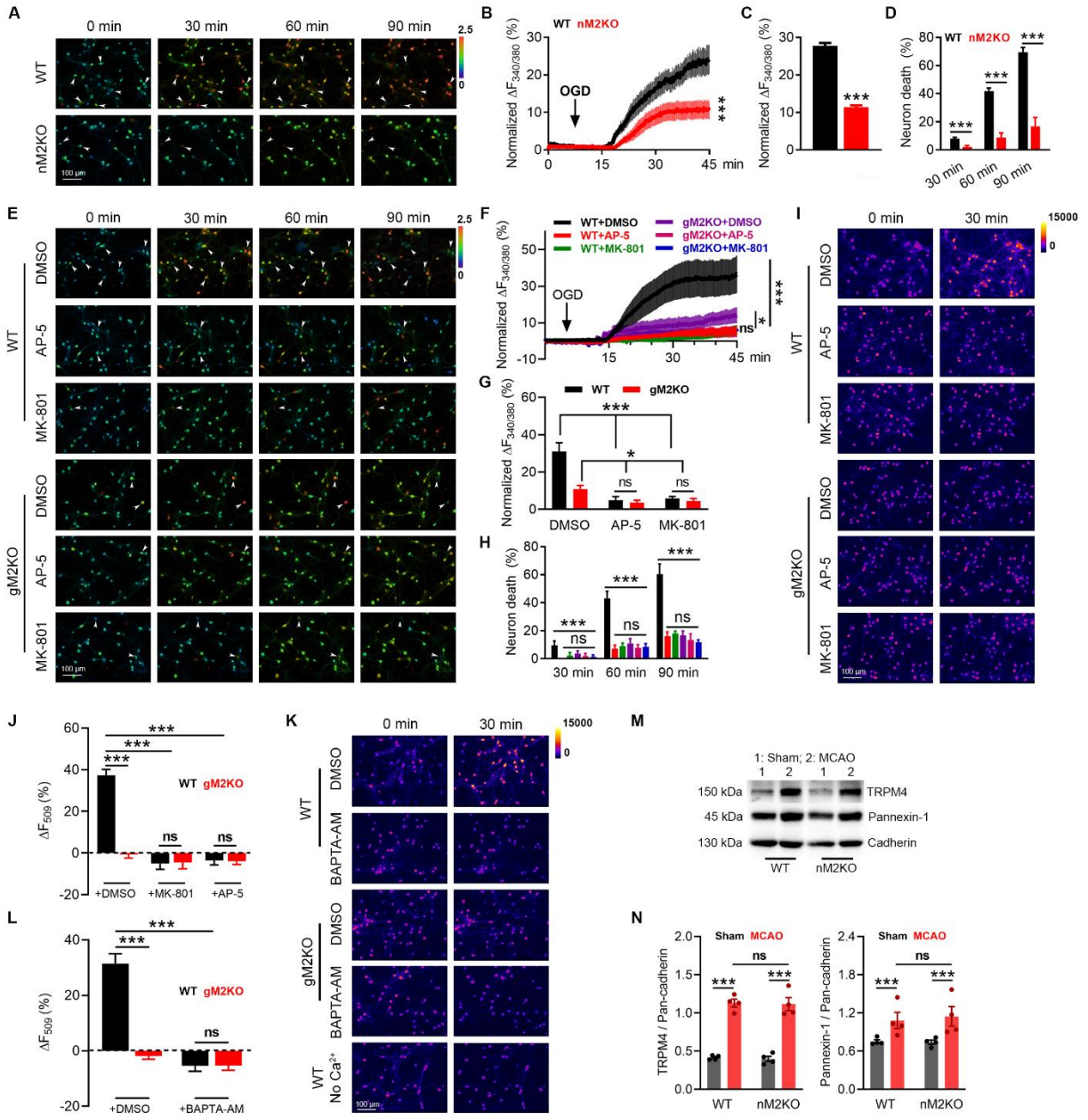


**Supplementary Figure 2 | Neuron-specific *Trpm2* Knockout (nM2KO) protects neurons from oxygen-glucose deprivation (OGD)-induced damage, Related to Figure 1**

(A), Evaluation of $Ca^{2+}$overload and neuronal death using Fura-2 real-time ratio $Ca^{2+}$ imaging. Cortical neurons were isolated from nM2KO mice (*Trpm2*$^{flox/flox}$, $Cre^{+}$) and WT littermate control mice (*Trpm2*$^{flox/flox}$, $Cre^{-}$) and cultured for 7 to 14 days. Neurons were exposed to OGD and intracellular $Ca^{2+}$ change was monitored by Fura-2 ratio $Ca^{2+}$ imaging for 90 mins. Neurons with increasingly elevated $Ca^{2+}$ levels, such as the ones indicated by arrows, died and disappeared at different time points. Ionomycin was used to

induce the maximum $Ca^{2+}$ influx for normalization (not shown).

(B), Representative sample traces of Fura-2 real-time $Ca^{2+}$ imaging normalized to ionomycin-induced responses. Averaged traces from 20 neurons which were randomly chosen from WT and nM2KO groups for analysis. Ionomycin was used to induce the maximum $Ca^{2+}$ influx for normalization (***, $p < 0.001$, unpaired *t*-test, mean ± SEM).

(C), Quantification of OGD-induced $Ca^{2+}$ changes after OGD for 30 min. 238 neurons from 3 WT mice in 6 culture dishes and 233 neurons from nM2KO mice in 6 culture dishes were used for analysis (***, $p < 0.001$, unpaired *t*-test, mean ± SEM).

(D), Quantification of OGD-induced neuronal death at 30, 60, and 90 min after OGD (***, $p < 0.001$, unpaired *t*-test, mean ± SEM). Neuronal death was monitored as $F_{340/380}$ fluorescence gradually reduced and eventually disappeared after the fluorescence reached maximal level (see representative dead cells indicated by arrows in (A)).

(E), Evaluation of $Ca^{2+}$overload and neuronal death using Fura-2 real-time ratio $Ca^{2+}$ imaging. Cortical neurons were isolated from WT and gM2KO mice and cultured for 7 to 14 days. During OGD, either DMSO, NMDAR channel blocker MK-801 or NMDAR antagonist AP-5 was applied. Neurons were exposed to OGD and intracellular $Ca^{2+}$ change was monitored by Fura-2 ratio $Ca^{2+}$ imaging for 90 mins. Neurons with increasingly elevated $Ca^{2+}$ levels, such as the ones indicated by arrows, died and disappeared at different time points. Ionomycin was used to induce the maximum $Ca^{2+}$ influx for normalization (not shown).

(F), Representative sample traces of Fura-2 real-time $Ca^{2+}$ imaging normalized to ionomycin-induced responses. Averaged traces from 10 neurons which were randomly chosen from each group for analysis. Ionomycin was used to induce the maximum $Ca^{2+}$ influx for normalization (***, $p < 0.001$, unpaired *t*-test, mean ± SEM).

(G), Quantification of OGD-induced $Ca^{2+}$ changes after OGD for 30 min. 20 ~ 30 neurons from each group were used for analysis (***, $p < 0.001$, unpaired *t*-test, mean ± SEM).

(H), Quantification of OGD-induced neuronal death at 30, 60, and 90 min after OGD (ns, $p > 0.05$, ***, $p < 0.001$, unpaired *t*-test, mean ± SEM). Neuronal death was monitored as $F_{340/380}$ fluorescence gradually reduced and eventually disappeared after the fluorescence reached maximal level (see representative dead cells indicated by arrows in (A)).

(I-J), Cultured cortical neurons from gM2KO and WT control littermates were subjected to OGD with the treatment of either DMSO, NMDAR channel blocker MK-801 or NMDAR antagonist AP-5. (I), R123 fluorescence changes in neurons of different groups induced by OGD. (J), Mean R123 fluorescence changes induced by 30 min OGD exposure. ~20 neurons from each group were randomly chosen from each group for quantification. The accumulated numbers of neurons in each group for data analysis were from 3~5 independent experiments using neurons isolated from 3 mice/group (ns, $p > 0.05$, ***, $p < 0.001$; ANOVA, Bonferroni's test; mean ± SEM).

(K-L), Cultured cortical neurons from gM2KO and WT control littermates were subjected to OGD with the treatment of either DMSO or BAPTA-AM, an intracellular $Ca^{2+}$ chelator. (I), R123 fluorescence changes in neurons of different groups induced by OGD. (J), Mean R123 fluorescence changes induced by 30 min OGD exposure. ~20 neurons from each group was randomly chosen from each group for quantification. The accumulated numbers of neurons in each group for data analysis were from 3~5 independent experiments using neurons isolated from 3 mice/group (ns, $p > 0.05$, ***, $p < 0.001$; ANOVA, Bonferroni's test; mean ± SEM).

(M-N) Global *Trpm2* deletion does not inhibit the increased surface expression of TRPM4 and pannexin-1 after MCAO. Representative images and quantification of WB bands of TRPM4 and pannexin-1. Pan-cadherin was used as a loading control (ns, $p > 0.05$, ***, $p < 0.001$; ANOVA, Bonferroni's test; mean ± SEM).

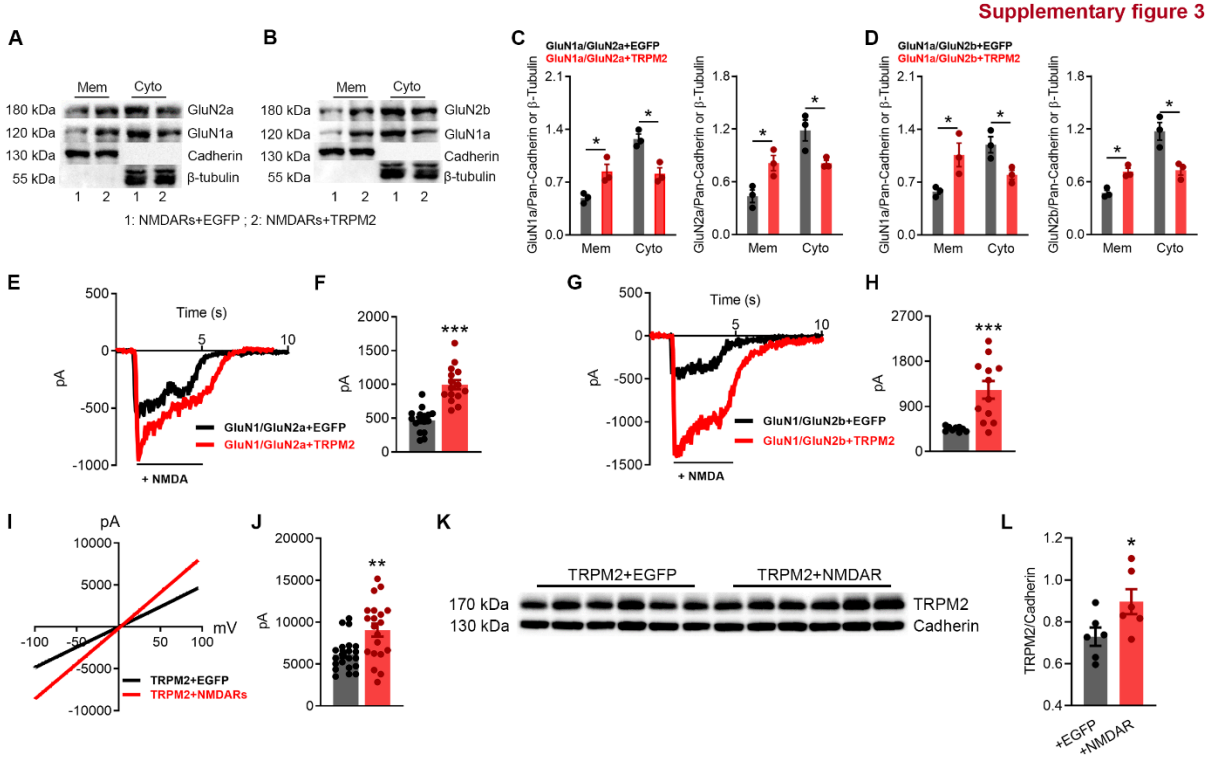


**Supplementary Figure 3 | TRPM2 increases both GluN1a/GluN2a and GluN1a/GluN2b surface expression levels, Related to Figure 2**

(A, C), Surface expression of GluN1a and GluN2a in HEK293T cells co-expressing EGFP (Con) or TRPM2 (+M2). (A), WB analysis of membrane and cytosol levels of GLuN1a and Glu2a. Pan-cadherin and β-tubulin were used as loading controls. (C), Quantification of GluN1a, GluN2a membrane (Mem) and cytosol (Cyto) expression (*, $p < 0.05$, **, $p < 0.01$; unpaired *t*-test, mean ± SEM, n=3).

(B, D) Surface expression of GluN1a and GluN2b in HEK293T cells co-expressing EGFP (Con) or TRPM2 (+M2). (B), WB analysis of membrane and cytosol levels of GluN1a and GluN2b. Pan-cadherin and β-tubulin were used as loading control. (D), Quantification of GluN1a, GluN2b membrane (Mem) and cytosol (Cyto) expression (*, $p < 0.05$, **, $p < 0.01$; unpaired *t*-test, mean ± SEM, n=3).

(E-F) Representative GluN1a/GluN2a currents (E) recorded in HEK-293T cells co-expressing GluN1a/GluN2a/EGFP or GluN1a/GluN2a/TRPM2, and mean current amplitude (F) (***, $p < 0.001$; ANOVA, Bonferroni's test; mean ± SEM, n=11~12).

(G-H) Representative GluN1a/GluN2b currents (G) recorded in HEK-293T cells co-expressing GluN1a/GluN2a/EGFP or GluN1a/GluN2a/TRPM2, and mean current amplitude (H) (***, $p < 0.001$; ANOVA,

Bonferroni’s test; mean ± SEM, n=11~12).

(I, J), Representative TRPM2 current traces and quantification of current amplitude recorded in HEK-293T cells transfected with TRPM2 with either EGFP or NMDARs (**, $p < 0.01$; ANOVA, Bonferroni’s test; mean ± SEM, n=15~20).

(K, L), Representative WB band and quantification of TRPM2 surface expression in HEK-293T cells transfected with TRPM2 with either EGFP or NMDARs (*, $p < 0.05$; ANOVA, Bonferroni’s test; mean ± SEM, n=15~20).

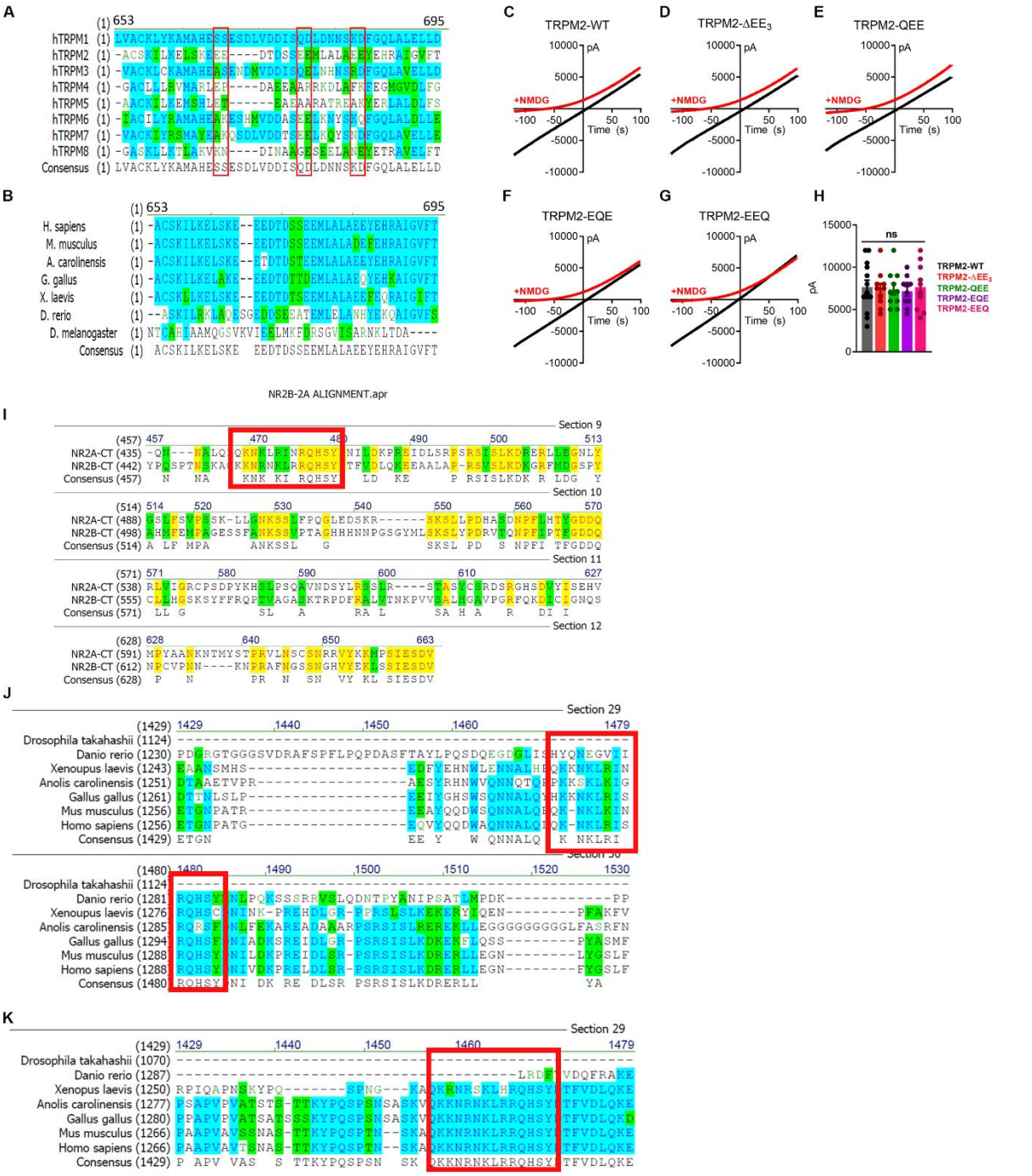


**Supplementary Figure 4 | Alignments of triple glutamate-glutamate repeats ($EE_3$) and functional evaluation of TRPM2-$EE_3$ domain mutants, and alignments of KKR domains in GluN2a and GluN2b, , Related to Figure 3 and 4**

(A, B), Alignment of triple EE domain ($EE_3$) in TRPM subfamily (A), and $EE_3$ domain in TRPM2 of different species (B).

(C-G), Representative TRPM2 current recordings from HEK-293T cells transfected with $EE_3$ domain deleted TRPM2 (TRPM2-$\Delta EE_3$) and TRPM2 mutants (QEE: E666Q, E667Q; EQE: E673Q, E674Q; EEQ: E680Q, E681Q).

(H), Quantification of TRPM2 current recording from HEK-293T cells transfected with different TRPM2 mutants. 10 recordings from each group were used for analysis (ns, $p>0.05$; ANOVA, Bonferroni's test; mean ± SEM).

(I), Alignment of KKR domain in GluN2a and GluN2b.

(J), Alignment of KKR domain in GluN2a in different species.

(K), Alignment of KKR domain in GluN2b in different species.

Supplementary figure 5

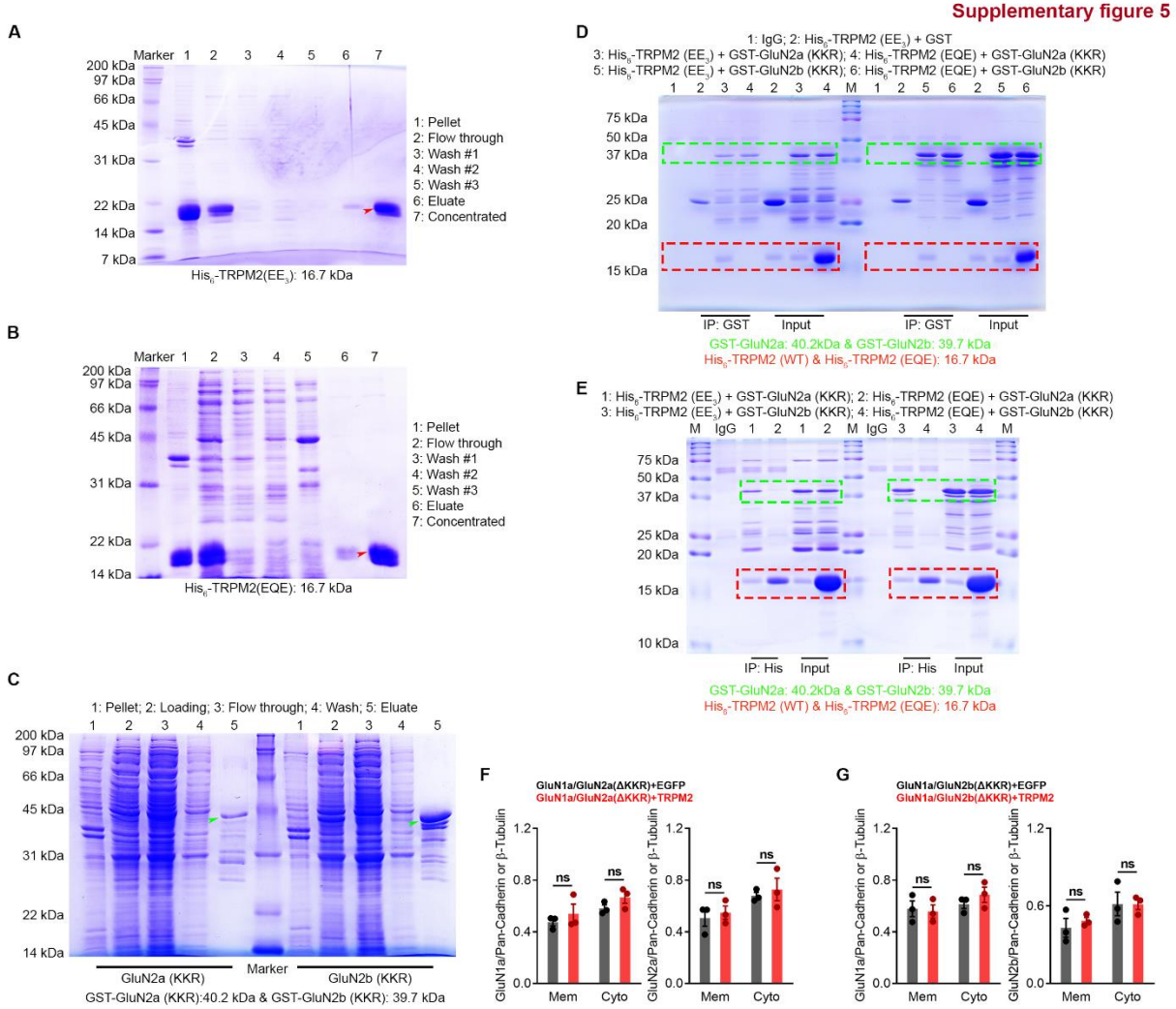


**Supplementary Figure 5 | Expression and purification of $EE_3$ containing fragments derived from TRPM2 and KKR containing fragments derived from GluN2a or GluN2b, Related to Figure 4**

(A, B), Coomassie blue stained SDS-PAGE gels showing the expression and purification process of $EE_3$ (A) or EQE (B) containing protein fragment derived from wild-type TRPM2 or its EQE mutant. The band with the expected molecular weight for the protein is indicated with a red arrow.

(C), Coomassie blue stained SDS-PAGE gel showing the expression and purification process of KKR containing protein fragment derived from GluN2a (left) or GluN2b (right). The band with the expected molecular weight for the protein is indicated with a green arrow.

(D), Coomassie blue stained SDS-PAGE gel showing the IP of the GST-tagged $EE_3$ or EQE fragments incubated with the $His_6$-tagged KKR fragments from either GluN2a (left) or GluN2b (right). The same samples were used in Figure 4E and F (right). Note that mutation of EEE to EQE abolished the binding.

(E), Coomassie blue stained SDS-PAGE gel showing the IP of the $His_6$-tagged KKR fragments from either GluN2a (left) or GluN2b (right) incubated with the GST-tagged $EE_3$ or EQE fragments.

(F, G), Quantification of the surface expression of GluN2a-ΔKKR and GluN2b-ΔKKR as shown in Fig 4G and Fig 4H, respectively (ns, $p>0.05$; ANOVA, Bonferroni's test; mean ± SEM).

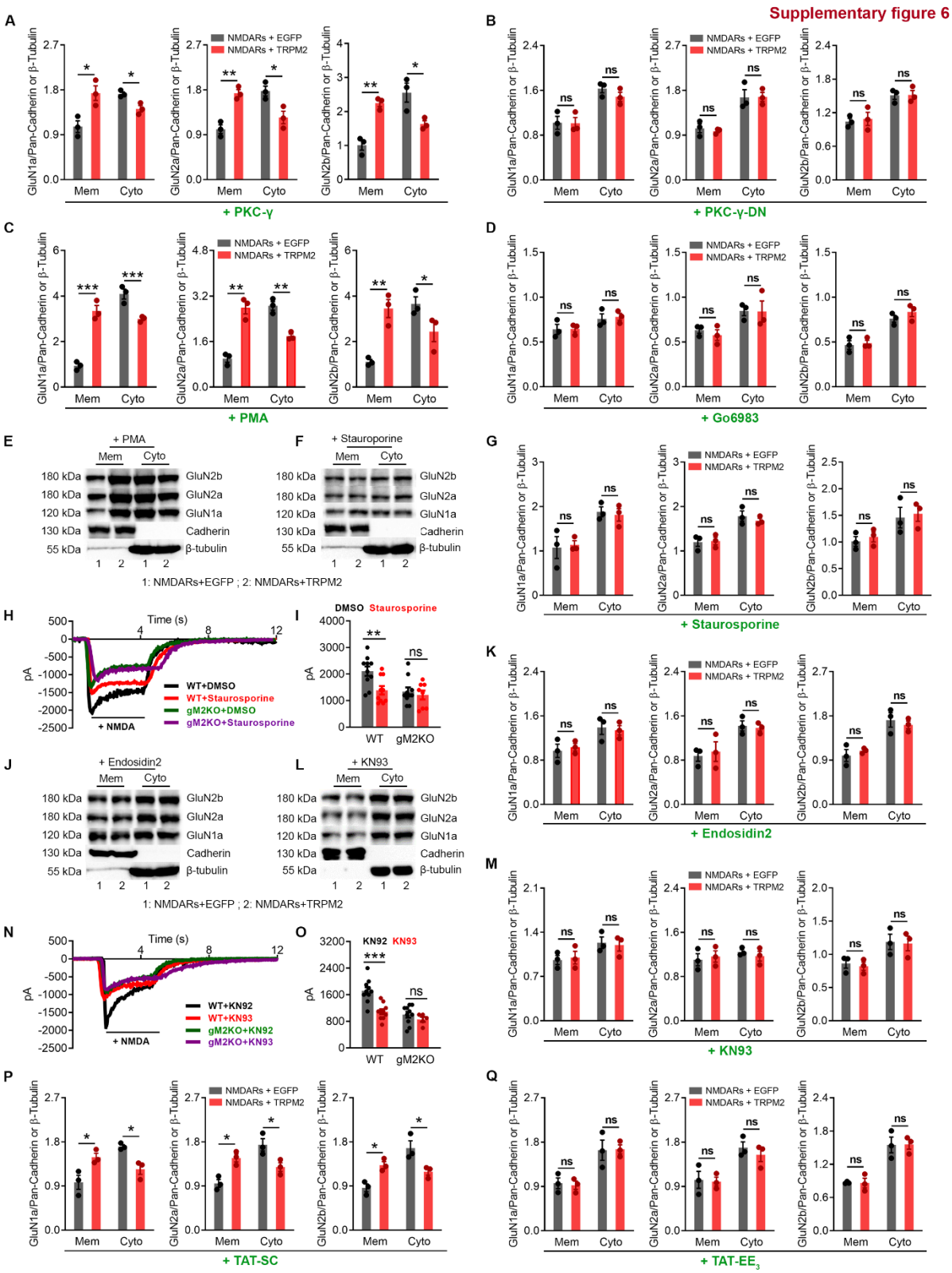


**Supplementary Figure 6 | Effects of staurosporine, endosidin2 and KN93 on surface expression levels of NMDARs. , Related to Figure 4, 5 and 6**

(A), Quantification of the surface expression of GluN1a, GluN2a, and GluN2b in cell membrane (Mem) and cytosol (Cyto) as show in Fig 5G (*, p< 0.05, **, p< 0.01; unpaired *t*-test; mean ± SEM, n=3).

(B), Quantification of the surface expression of GluN1a, GluN2a, and GluN2b in cell membrane (Mem) and cytosol (Cyto) as show in Fig 5H (ns, p>0.05; unpaired *t*-test; mean ± SEM, n=3).

(C), Quantification of the surface expression of GluN1a, GluN2a, and GluN2b in cell membrane (Mem) and cytosol (Cyto) as show in Fig 5I (*, p< 0.05, **, p< 0.01, ***, p< 0.001; unpaired *t*-test; mean ± SEM, n=3).

(D), Quantification of the surface expression of GluN1a, GluN2a, and GluN2b in cell membrane (Mem) and cytosol (Cyto) as show in Fig 5J (ns, p>0.05; unpaired *t*-test; mean ± SEM, n=3).

(E), Representative Western blot bands with a bit over-saturation of the NMDARs+TRPM2 group for better showing the surface expression level in the NMDARs+EGFP group. Notice the marked difference between the NMDARs+EGFP group and the NMDARs+TRPM2 group.

(F, G), Surface expression of NMDARs in HEK-293T cells co-transfected with TRPM2 or EGFP with the treatment of PKC inhibitor Staurosporine. Membrane (Mem) and cytosol (Cyto) NMDARs were quantified from 3 independent experiments (G) (ns, p > 0.05, unpaired *t*-test, mean ± SEM, n=3/group).

(H, I), Effects of PKC inhibitor Staurosporine on NMDAR currents recorded from cortical neurons cultured for 14 days. (H), Representative NMDAR currents elicited at -80 mV by 10 μM NMDA in WT and TRPM2-KO (gM2KO) neurons treated with or without Staurosporine at 1 μM for overnight. (I), Mean current amplitude (ns, p>0.05; **, p < 0.01; ANOVA, Bonferroni's test; mean ± SEM, n=10~15 neurons from 2 mice, respectively).

(J, K), Surface expression of NMDARs in HEK-293T cells co-transfected with TRPM2 or EGFP with the treatment of exocytosis inhibitor Endosidin2. Membrane (Mem) and cytosol (Cyto) NMDARs were quantified from 3 independent experiments (K) (ns, p > 0.05, unpaired *t*-test, mean ± SEM, n=3/group).

(L, M), Surface expression of NMDARs in HEK-293T cells co-transfected with TRPM2 or EGFP with the treatment of CaMKII inhibitor KN93. Membrane (Mem) and cytosol (Cyto) NMDARs were quantified from 3 independent experiments (M) (ns, p > 0.05, unpaired *t*-test, mean ± SEM, n=3/group).

(N, O), Effects of CaMKII inhibitor KN93 on NMDAR currents recorded from cortical neurons cultured for 14 days. (N), Representative NMDAR currents elicited at -80 mV by 10 μM NMDA in WT and TRPM2-KO (gM2KO) neurons treated with KN93 or negative control KN92 at 10 μM for overnight. (O), Mean current

amplitude (ns, p>0.05; **, p < 0.01; ANOVA, Bonferroni's test; mean ± SEM, n=10~15 neurons from 2 mice, respectively).

(P), Quantification of the surface expression of GluN1a, GluN2a, and GluN2b in cell membrane (Mem) and cytosol (Cyto) as show in Fig 6C (*, p< 0.05; unpaired *t*-test; mean ± SEM, n=3).

(Q), Quantification of the surface expression of GluN1a, GluN2a, and GluN2b in cell membrane (Mem) and cytosol (Cyto) as show in Fig 6D (ns, p>0.05; unpaired *t*-test; mean ± SEM, n=3).

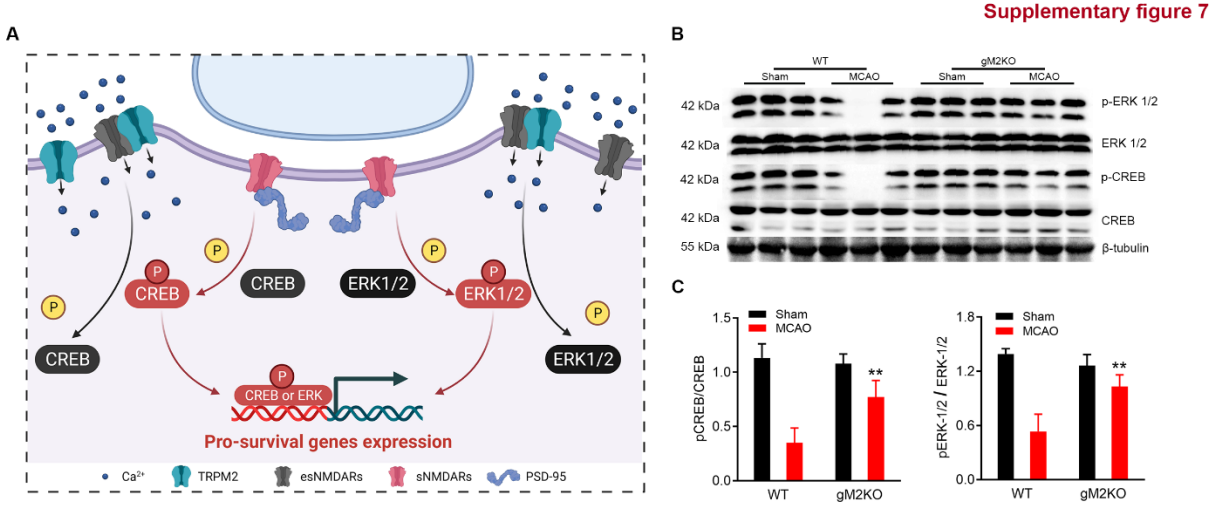


**Supplementary Figure 7 | Global TRPM2 Knockout preserves CREB and ERK-1/2 signaling after MCAO, Related to Figure 7**

(A), Graphic illustration of the pro-survival pERK1/2 and pCREB signaling downstream of synaptic NMDARs. PSD-95 is a synaptic marker and is associated with synaptic NMDARs. Were TRPM2 expressed on the post-synaptic membrane, anti-PSD-95 should be able to immunoprecipitate TRPM2 (Figure 7U). Moreover, there was extremely low TRPM2 abundance in the synaptosome isolation (Figure 7V).

(B), Western blotting analysis of changes of p-ERK 1/2, ERK-1/2, p-CREB, and CREB expression in the brain from WT and TRPM2-KO subjected to sham or MCAO surgery.

(C), Quantification of pERK-1/2 and pCREB after MCAO or sham surgery. Four mice from each group were used for quantification (**, $p < 0.01$; ANOVA, Bonferroni's test; mean ± SEM, n=4/group).

**Table S1. Primers for subcloning, mutagenesis and genotyping , Related to SRAR Methods.**

| Application | Genes | Primers | Primer sequences (5'-3') |
|---|---|---|---|
| Subcloning | *Trpm2* C terminal part | F | CTCGAATTCTGAAGGAGAACTACCTCCAGAAC |
| | | R | GATCTAGATTAGGTCTTGTGGTTCGCATAGAGTG |
| | *GluN2a* C terminal part | F | CGGAATTCCGACACTCTTCTACTGGAAG |
| | | R | TGCTCTAGAGCTTAAACATCAGATTCGATACTAGG |
| | *GluN2b* C terminal part | F | CGGAATTCCGTCATCACCTTCATCTGTGAG |
| | | R | TGCTCTAGAGCACCTTAACCTCTCTCTCTTC |
| Mutagenesis | *Trpm2* 1-727 | F | CAAGGACATGTAGTTTGTGTC |
| | | R | GACACAAACTACATCATGTCCTTG |
| | *Trpm2* 1-679 | F | TGGCGCTGGCGTAGTAGTATG |
| | | R | TCATACTACTACGCCAGCGCC |
| | *Trpm2* 1-631 | F | ATTTGGGCCATTGTCTAGAACCGT |
| | | R | ACGGTTCTAGACAATGGCCCAAATG |
| | *Trpm2* 1-570 | F | TGCTGGGGGAATTCACGCAG |
| | | R | TGCGTGAATTCCCCCAGCAG |
| | *Trpm2* 1-664 | F | TGAAGGAACTGTCCTAGGAGGAGGAG |
| | | R | TCCTCCTCCTAGGACAGTTCCTTCAG |
| | *Trpm2* $EE_3$ deletion | F | AAGATCCTGAAGGAACTGTCCAAGTATGAGCACAGAGCCATC |
| | | R | GATGGCTCTGTGCTCATACTTGGACAGTTCCTTCAGGATCTT |
| | *Trpm2* QEE | F | AAGGAACTGTCCAAGCAGCAGGAGGACACGGAC |
| | | R | TCCGTGTCCTCCTGCTGCTTGGACAGTTCCTTC |
| | *Trpm2* EQE | F | ACACGGACAGCTCGCAGCAGATGCTGGCG |
| | | R | CGCCAGCATCTGCTGCGAGCTGTCCGTGTC |
| | *Trpm2* EEQ | F | TGGCGCTGGCGCAGCAGTATGAGCACAGAG |
| | | R | TCTGTGCTCATACTGCTGCGCCAGCGCCAG |

| | | | |
|---|---|---|---|
| | *GluN2a* 1-1053 | F | ACCTTCATCTGGTAGCACCTCTTCTAC |
| | | R | TAGAAGAGGTGCTACCAGATGAAGGTG |
| | *GluN2b* 1-1047 | F | ACCTTCATCTGTTAGCATCTGTTCTATTG |
| | | R | AATAGAACAGATGCTAACAGATGAAGGTG |
| | *GluN2a* KKR deletion | F | TATGATAACATTCTGGACAAACCCAG |
| | | R | GAACTGGAGGGCGTTGTT |
| | *GluN2b* KKR deletion | F | TCCTACGACACCTTCGTG |
| | | R | CTGAGCCTTGGAATTAGTCGG |
| *E.coli* expression | | | |
| | *Trpm2* $EE_3$ | F | ATATGCGGCCGCTCAGGCCATGTGACCTTCAC |
| | | R | ATATGGTACCTTACTTCATGTCCTTGGCCTCCAG |
| | *Trpm2* EQE | F | ATATGCGGCCGCTCAGGCCATGTGACCTTCAC |
| | | R | ATATGGTACCTTACTTCATGTCCTTGGCCTCCAG |
| | *GluN2a* KKR | F | ATATGCGGCCGCTCTCCTTTCAAGTGTGATGC |
| | | R | ATATGGTACCTTAGCT TTTGTTCCCCAAGAGTTT |
| | *GluN2b* KKR | F | ATATGCGGCCGCGAGGCCTGTAAGAAGGCT |
| | | R | ATATGGTACCTTATGAGGACTTGTTGGCAAA G |
| Genotyping | *Cre* | F | GATATCTCACGTACTGACGG |
| | | R | TGACCAGAGTCATGGTTAGC |
| | *Trpm2 loxp* | F | GGCTCTGCCTCATCCCCAGAATC |
| | | R | CCGGATACAGATGCAGGATGCTG |
| | | R | CTGAAGGTCCTGAGTTTGAATCCCA |
| | TRPM2-KO | F | CTTGGGTTGCAGTCATATGCAGGC |
| | | R | GCCCTCACCATCCGCTTCACGATG |
| | | R | GCCACACGCGTCACCTTAATATGC |